2023-10

A climate perturbation at the Middle Late Jurassic Transition? Evaluating the isotopic evidence from south-central England

Watanabe, Sayaka

10.1016/j.palaeo.2023.111755
Palaeogeography, Palaeoclimatology, Palaeoecology
Elsevier BV

A climate perturbation at the Middle –Late Jurassic Transition? Evaluating the isotopic evidence.

Gregory D. Price*[1], Bernát Heszler[1,2], Lauren-Marie Tansley Charlton[1], Jade Cox[1]

[1]School of Geography, Earth and Environmental Sciences

University of Plymouth, Plymouth, UK, PL4 8AA

[2] Department of Geology, Eötvös Loránd University, Pázmány Péter sétány 1/C,

Budapest H-1117, Hungary

*Corresponding author

Abstract The Jurassic greenhouse is punctuated by short cooling intervals with at times postulated polar ice-sheet development. Published oxygen isotope records of belemnite rostra and fish teeth have been interpreted to reveal a prominent decrease in seawater temperature during the Late Callovian–Early Oxfordian. This is in part the basis for a proposed an ice age at the Middle-Late Jurassic Transition. In contrast relatively constant oxygen isotope records and therefore seawater temperatures and carbon isotope values characterized by significant scatter but showing more positive values during the middle and late Callovian have been reported from elsewhere. This research has constructed a stable isotope stratigraphy (from belemnites, Gryphaea and oysters) principally from the Callovian-Oxfordian interval (from southern England) and integrated these data with existing data to assess the pattern of carbon and oxygen isotopic change. Our marine

macrofossil record reveals isotopic patterns that are generally comparable with other European basins. Carbon isotopic trends are consistent with bulk carbonate carbon isotope records displaying systematic fluctuations, the largest of which (Middle Callovian, Calloviense/Jason Zones to Early Oxfordian, Mariae Zone) corresponds to previously identified phases of environmental perturbation. Such a trend may have resulted from enhanced burial and preservation of organic matter, leaving the seawater more positive in terms of carbon. Inferred cooling, derived from our oxygen isotope data from southern England, occurs within the Late Callovian and Oxfordian (Athleta to Mariae zones). Cooling post-dates this positive carbon isotope excursion. Enhanced carbon burial and atmospheric carbon dioxide draw down may have induced cooling. In this study the analysis of a single region (southern England) allows some constraints on potential variables that may influence isotope records. If Jurassic polar climates were truly warm such a degree of cooling would undoubtedly lead to cooler polar temperatures – but only with seasonal ice.

Key words: Dorset; Jurassic; Callovian; Oxfordian; carbon and oxygen isotopes; belemnites, Gryphaea; oysters

1. Introduction

The Jurassic greenhouse is punctuated by short cooling intervals with at times postulated polar ice-sheet development (Dromart et al., 2003; Dera et al., 2011; Donnadieu et al. 2011; Nordt, et al., 2021). These cold intervals have been classically attributed to a transient atmospheric CO_2 drawdown. For example, late Pliensbachian and early Toarcian expanding polar ice caps, global cooling and sea level variations have been linked to carbon cycle changes (Krenker et al. 2019; Ruebsam and Al-Husseini 2021). Likewise, cooling and a proposed an ice age at the Middle-Late Jurassic (Late Callovian–Early Oxfordian) transition has been linked to reduced CO_2 (Dromart et al., 2003) and evidenced through oxygen isotope records of belemnite rostra and fish teeth from the Russian Platform, eastern France and western Switzerland (e.g., Barskov and Kiyashko, 2000; Dromart et al., 2003; Lécuyer et al., 2003). In contrast relatively constant oxygen isotope records and therefore seawater temperatures and $\delta^{13}C$ values characterized by significant scatter but showing more positive values during the middle and late Callovian have been reported from central Poland, Russia and India (Wierzbowski et al., 2009; Alberti et al., 2012). Global cooling and the presence of major continental ice caps during the Jurassic continues to be the subject of debate (e.g., Korte and Hesselbo, 2011; Wierzbowski and Rogov, 2011; Krencker et al., 2019; Ruebsam and Al-Husseini 2021). The aim of this research is to describe and evaluate a stable isotope stratigraphy from the Callovian-Oxfordian interval and integrate these data with existing isotopic records to assess the pattern of carbon and oxygen isotopic changes. Through analysis of a single region (southern England) allows some constraints on potential variables that may influence isotope records to be fully assessed.

2. Geological Setting and Sampling Locations

63 During the Middle to Late Jurassic Europe was flooded by a shallow epeiric sea (Fig. 1).
64 Britain's palaeolatitude (40°N), placed it directly between the carbonate platform of the Tethys
65 Ocean, the proto-Atlantic and the Boreal Sea siliciclastic dominated sequences with faunas being
66 typically intermediate between the two (Price and Page, 2008; Wierzbowski et al., 2013; Pellenard
67 et al., 2014; Cope, 2016). Southern England consisted of partly emergent land masses, namely the
68 London-Brabant Massif to the east, the Armorican Massif to the south and the smaller Cornubian
69 and Welsh Massif's to the west. As detailed below, belemnite, oyster and Gryphaea samples were
70 collected from multiple locations across Dorset, Wiltshire and Cambridgeshire, UK (Figs 1-3).

71 2.1 Burton Cliff, Burton Bradstock, Inferior Oolite

72 The oldest samples examined is this study come from the Bajocian Inferior Oolite at Burton Cliff,
73 Burton Bradstock, Dorset, UK (Fig. 2). These are bioturbated and fossiliferous limestones (Callomon
74 and Cope, 1995; Cope, 2016). Samples were collected from the Snuff-boxes, the Red Conglomerate
75 Bed and Beds 13 and 14. The Snuff-boxes horizon is marly, blue grey oolitic limestone, with
76 ellipsoidal, laminated oncolytic biscuits ('snuff-boxes') (Palmer and Wilson 1990; Callomon and
77 Cope, 1995). Ammonites previously identified represent the Discites Zone. The Red Conglomerate
78 bed comprises of ironshot, chamositic oolites, spanning the Humphriesianum and Subfuracatum
79 Zones (Callomon and Cope, 1995). Bed 13 (the Truellei Bed) is marly limestone and with scattered
80 ooids and contains ammonites from the Parkinsoni Zone, Truelli Subzone (Callomon and Cope,
81 1995). Bed 14 is a limestone with echinoderms, large nautiloids, brachiopods, sponges and bivalves.
82 Ammonites include *Parkinsonia bombfordi* (Parkinsoni zone, bombfordi Subzone) (Callomon and
83 Cope, 1995).

84 2.2 Kellaways, River Avon, Kellaways Sand Member

Callovian samples were derived from the type locality of the Kellaways Formation (Page, 1989), located on the river Avon, west of Tytherton, Wiltshire, UK. Although the exposure is limited (Fig. 2), the basal Kellaways Clay Member is overlain by the Kellaways Sand Member, consisting of bioturbated silts and calcareous sands (Page, 1989; Hudson and Martill, 1991). Fossils include ammonite's representative of the Calloviense Subzone, belemnites (*Cylindroteuthis*) and benthic bivalves (Page, 1989; Hudson and Martill, 1991).

2.3 Yaxley Clay Pit, Cambridgeshire, Peterborough Member

At Yaxley, Cambridgeshire, the Peterborough Member (Jason Zone) of the Oxford Clay formation is exposed in a former clay pit (Hudson and Martill, 1991) and contains crushed aragonitic ammonites, belemnites and gryphaea. Belemnites (*H. Hastata*) and Gryphaea (*G. dilobotes*) samples were obtained from Yaxley.

2.4 Fleet Lagoon, Dorset, Oxford Clay

Belemnite, oyster and Gryphaea samples were obtained from exposures at Tidmoor Point and Furzedown, Fleet Lagoon, Dorset. At Tidmoor Point the Oxford Clay, Lamberti Zone (Callomon and Cope 1995) comprises of bioturbated calcareous clays and includes *Kosmeroceras* and *Quenstedtoceras* and other abundant fossils including the large *Gryphaea lituola* and belemnites (including *H. hastata)* (Callomon and Cope, 1995; Cope, 2016). Belemnite (*H. hastata*) and Gryphaea (*G. lituola*) samples were also obtained from the Furzedown Clay Member (Mariae Zone, Scarburgense subzone, Wright, 1986), Oxford Clay at Furzedown of the Dorset, Fleet (Arkell 1947).

2.5 Redcliff Point, Dorset, Oxford Clay

Belemnite and Gryphaea samples were obtained from Redcliff Point near Weymouth, Dorset (Fig. 2), where a Callovian-Oxfordian boundary succession is exposed (Arkell, 1947; Wright, 1986). The

section has consequently been proposed as a candidate GSSP for the base of the latter stage. The samples were obtained from the Weymouth Member (Lamberti and Scarburgense Zones and subzones). The Weymouth member consist of a relatively hard medium to pale grey claystones and marls and were deposited in waters reaching a few tens of metres in depth (Hudson and Martill, 1991). The succession also contains the belemnite *H. hastata,* generally uncommon oxytomid bivalves and *G.* ex grp *dilatata*. Of these, belemnites (*H. hastata*); and Gryphaea (*G.* ex grp *dilatata*) were analysed.

2.6 Sandridge Park, Wiltshire, Sandridge Member

The principal exposure, type locality and sampling location of the Sandridge Member, is at the Sahara Sand Quarry (Sandridge Pit, Melksham Quarry, Wiltshire), comprising of a cross-bedded shelly and bioturbated shelly sands (Wright, 2014). This large sand pit is now a landfill site, with limited exposure. Bed 2 is the only remaining unit left exposed, a tempestite deposit, consisting of coarse-grained bioturbated shelly sands (Wright, 2014). The fossils derived from this location include *Liostrea*. The Sandridge Member belongs to the Cordatum Zone (Cordatum Subzone, Wright, 2014).

2.7 Sandsfoot Castle, Weymouth, Sandsfoot Grit Member

Belemnite and oyster (*Deltoideum delta*) samples were collected from the Sandsfoot Grit Member (Pseudocordata Zone (Regulare-Rosenkrantzi), Pseudoyo subzone, Wright 1986) from cliffs exposed beneath Sandsfoot Castle, Dorset (Fig. 2). Here the sediments consist of bioturbated sandy ironstones with chamosite ooids suggesting shallow, high energy deposition (Cope, 2016).

3. **Methodology**

Optical microscopy and cathodoluminescence (CL) analysis, in conjunction with elemental geochemistry, was undertaken in order to determine the state of preservation of each fossil specimen examined. Polished thin sections were prepared from representative specimens collected from each locality. CL was undertaken using a CITL Mk5-2 luminescence model, coupled with a Nikon Eclipse 50iPOL microscope. For elemental geochemistry and stable isotopes, calcite fragments judged to be best preserved were selected. The criteria being transparent honey coloured calcite, avoiding any dark brown or frosted fragments. Weighed calcites were dissolved in nitric acid and elemental concentrations (Ca, Mg, Sr, Mn and Fe) were generated using a Thermo Scientific iCAP 7000 Plus Inductively Coupled Plasma Optical Emission Spectrometer (ICP-OES) at the University of Plymouth. The reference material JLs-1 Limestone was also included in the ICP-OES analysis. Stable isotope data were generated on a Thermo Scientific Delta V Advantage with a Gasbench II online gas preparation module at the Stable Isotope Laboratory, University of Plymouth. Isotope ratios were calibrated using NBS-19 standard and are given in δ notation relative to the Vienna Pee Dee Belemnite (VPDB). Reproducibility was typically better than 0.1‰ for all samples and standard materials.

4. **Results**

4.1 Petrographic and CL analysis

The belemnites were typically honey coloured typical of pristine primary calcite. Most of the diagenetic alteration observed occurred around the outer margins (Fig. 4) and in the apical regions revealing sparry calcite re-crystallisation (consistent with other studies, e.g., Price and Teece, 2010; Wierzbowski and Rogov, 2011; Mettam et al., 2014). Using CL, the belemnite rostra examined were in general non-luminescent. The main areas of luminescence were the outer shell margins and the apical regions and along any prominent cracks/microfractures.

Petrographic and CL analysis of the oyster specimens showed mostly non-luminescent, well-preserved foliated shells, representing primary calcite. The main areas of alteration identified were along the outer shell rims, along prominent fractures, within borings and within interspersed lens shaped chambers. These chambers are seen interspersed throughout the shell and were possibly previously occupied with porous chalky calcite (e.g., Banker and Sumner, 2020). For example, the samples from Tidmoor Point, and Sandsfoot Castle, show luminescent sparry calcite and infilled microborings along the outer margins, and cross cutting veins and spar in spaces within the shells. These areas (Fig. 5) were avoided during subsampling for stable isotopes. The Gryphaea samples were characterised by typical pristine branching cross foliation structures (e.g., Malchus and Aberhan, 1998) (Fig. 5) and were largely non-luminescent. Some evidence of diagenetic alteration was observed, with sparry calcite present on the shell margins. Some showed fractures infilled with matrix and luminescent sparry calcite re-crystallisation (Fig. 5).

4.2 Elemental Geochemistry

Element concentrations (Fe, Mn, Mg, Sr, and Ca) were obtained to assess the degree of diagenetic alteration (Appendix 1). Fe and Mn concentrations are typically higher in diagenetically altered calcite, as Fe^{2+} and Mn^{2+} are more soluble under reducing conditions and thus available for replacing Ca^{2+} in the calcite lattice (Brand and Veizer 1980). Increases in Mn and Fe are often mirrored by decreases in Mg and Sr. Bivalves (including oysters and Gryphaea) typically show more variable in Fe and Mn concentrations compared to belemnites (Anderson et al., 1994; Price and Page, 2008; Price and Teece, 2010). For belemnites, the Mg concentrations ranged between 903 and 5292 ppm (mean 2371 ppm), for Sr between 660 and 1819 (mean 1013 ppm) and 25.6 and 59.3% (mean 40.0%) for Ca. The total determined Mn and Fe values ranged between 2 and 548 ppm (mean 36ppm) for Mn, and between 30 and 1115 ppm (mean 190 ppm, excluding the single

very high value) for Fe (Appendix). Belemnite specimens with high concentrations of Mn (>150ppm) and Fe (>300 ppm) were determined to be possibly diagenetically altered (cf. Price and Teece, 2010; Wierbowski 2004; Ditchfield 1997) and were excluded from further analysis.

For the oysters and Gryphaea, the Mg concentrations ranged between 273 and 1249 ppm (mean 444 ppm), Sr between 401 and 807 (mean 574 ppm) and 24.0 and 52.8% (mean 41.0%) for Ca. Determined Mn and Fe values ranged between 6 and 207 ppm (mean 59 ppm) for Mn, and between 30 and 1115 ppm (mean 318 ppm) for Fe (Appendix). Bivalves (including Gryphaea and oysters) are typically characterized by quite variable Fe and Mn contents (e.g., Milliman, 1974; Anderson et al. 1994; Korte and Hesselbo, 2011; Price and Page 2008). The Gryphaea and oyster samples with high Fe and Mn concentration were excluded from further analysis. Overall, most belemnites, oysters and Gryphaea are deemed well preserved.

4.3 Oxygen isotopes

The well-preserved belemnite $\delta^{18}O$ values of this study display a modest variability, ranging between −2.1‰ and +0.7‰ (V-PDB) (averaging −0.5‰)(Fig. 6). These data have been combined with well-preserved belemnite calcite oxygen isotope data from Jenkyns et al. (2002); Price et al. (2009), Price and Page (2008), Price et al. (2015), Li et al. (2013), Anderson et al. (1994) and Price and Teece (2010) from the same region (see Figs. 1, 3). Stratigraphically, the $\delta^{18}O$ values show more positive values during the Bajocian, reaching +0.7‰ in the Parkinsoni zone (Truellei subzone)(Fig. 7). The $\delta^{18}O$ values then shift to more negative values during the Late Bajocian and the most negative values are seen within the Peterborough Member (Middle Callovian, Jason Zone). Subsequently the $\delta^{18}O$ values become more positive, reaching most positive values in the Late Callovian (Athleta Zone) and Early Oxfordian (Marie zone) (Fig. 7). A slight return to more negative

197 $\delta^{18}O$ values follows reaching the most negative (−1.3‰) in the Sandsfoot Grit Member (Oxfordian,
198 Pseudocordata Zone, Pseudoyo Subzone).

199 The oyster and Gryphaea $\delta^{18}O$ values (Fig. 6) of this study display a larger variability ranging
200 between −3.5‰ and +0.4‰ (V-PDB). The oyster and Gryphaea $\delta^{18}O$ values are slightly more
201 negative on average compared to the belemnite $\delta^{18}O$ values (similar to the pattern seen by Price
202 and Page, 2008; Mettam et al., 2014). These data have been combined with well-preserved
203 belemnite calcite oxygen isotope data from Hendry and Kalin (1997), Price and Teece (2010), Price
204 and Page (2008), Mettam et al. (2014), Anderson et al. (1994), Martin-Garin et al. (2010), Jenkyns et
205 al. (2002) and Price et al. (2009). The stratigraphic $\delta^{18}O$ trends, are similar to the belemnite data,
206 whereby $\delta^{18}O$ values show more positive values during the Bathonian, reaching +1.1‰ in the
207 Retrocostatum zone. The $\delta^{18}O$ values then shift to more negative values with the most negative are
208 seen within the Callovian (Calloviense Zone) at Kellaways and within Peterborough Member
209 (Callovian, Jason Zone). Subsequently the $\delta^{18}O$ values become more positive, reaching most
210 positive values in the Late Callovian (Lamberti Zone, Lamberti Subzone) at Redcliff Point (Fig. 8). A
211 return to more negative $\delta^{18}O$ values follows reaching the most negative (−3.5‰) in the Sandsfoot
212 Grit Member (Oxfordian, Pseudocordata Zone, Pseudoyo Subzone) and in the Kimmeridgian (the
213 data of Jenkyns et al. 2002).

214 4.4 Carbon Isotopes

215 The belemnite $\delta^{13}C$ values of this study (Fig. 6) displayed a relatively large variability, ranging
216 between −2.1‰ and +4.0‰ (V-PDB) (average +1.2‰). Combining with published data,
217 stratigraphically the $\delta^{13}C$ values show positive values during the Bajocian and then shift to more
218 negative values during the Bathonian (down to −2.3‰). Subsequently the $\delta^{13}C$ values become
219 much more positive, reaching the most positive values in the Callovian (Calloviense−Jason Zones) at

220 Kellaways. Positive values are maintained until the early Oxfordian reaching a maximum of +3.6‰
221 at Redcliff Point (Mariae Zone, Scarburgense Subzone). A return to more negative $\delta^{13}C$ values
222 follows reaching the most negative values (−0.5‰) in the Sandsfoot Grit Member (Oxfordian,
223 Pseudocordata Zone, Pseudoyo Subzone).

224 The oyster and Gryphaea $\delta^{13}C$ values (Fig. 6) of this study display a larger variability ranging
225 between +1.4‰ and +5.1‰ (V-PDB) (average +3.6‰). The oyster and Gryphaea $\delta^{13}C$ values are
226 more positive compared to the belemnite $\delta^{13}C$ values. The Gryphaea show the most positive values
227 (Fig. 6). These data have been combined with well-preserved oyster and Gryphaea calcite carbon
228 isotope data from Price and Teece (2010), Price and Page (2008), Mettam et al. (2014), Anderson et
229 al. (1994), Martin-Garin et al. (2010), Jenkyns et al. (2002) and Price et al. (2009). The stratigraphic
230 $\delta^{13}C$ trends, are similar to the belemnite data, whereby $\delta^{13}C$ values show moderately positive
231 values during the Bathonian, and then shift to more positive values within the Callovian
232 (Calloviense Zone) at Kellaways. Within Peterborough Member (Callovian, Jason Zone) positive
233 values are also seen although a considerable spread of values is observed. Positive carbon isotope
234 values are seen also in the Furzedown Clay Member (Oxfordian, Mariae Zone) (reaching +4.9 ‰). A
235 return to slightly less positive $\delta^{13}C$ values follows for the Sandridge Member (Oxfordian, Cordatum
236 Zone) and the remainder of the Oxfordian through into the Kimmeridgian.

237 **5. Discussion**

238 Belemnite, oyster and Gryphaea $\delta^{13}C$ values have been found to be a reliable proxy for
239 temporal changes of the isotope composition of the dissolved inorganic carbon (DIC) in ancient seas
240 (Anderson et al., 1994; Price et al., 2000; Rosales et al., 2001; Wierzbowski, 2004; Wierzbowski and
241 Joachimski, 2007; Price and Teece, 2010; Mettam et al., 2014). The observed scatter of coeval $\delta^{13}C$
242 values of belemnite rostra and oysters and Gryphaea shells may result from short-lived temporal

changes in the isotope composition of the DIC in the ambient waters. Variations in biologic productivity as well as mixing of different DIC sources into the shallow middle and late Jurassic seas may account for some of these the temporal changes. The differences between the $\delta^{13}C$ values of belemnites, oysters and Gryphaea (Fig. 6) suggests that one or both groups may have been characterized by a different metabolic effect and/or differences linked to variation in ambient DIC associated with habitat. Nevertheless, both groups show comparable carbon trends through the examined interval.

A large positive carbon isotope shift seen in the middle Callovian (Calloviense-Jason Zones) and positive values are maintained until the early Oxfordian (Mariae Zone, Scarburgense Subzone). Such a trend may have resulted from enhanced burial and preservation of organic matter (e.g., Weissert, 1989), leaving the seawater more positive in terms of $\delta^{13}C_{seawater}$. Dromart et al. (2003) for example identify Callovian organic-rich deposits including the Peterborough Member (Calloviense-Jason Zones) of the Oxford Clay Formation in England (Kenig et al., 1994), and the Tuwaiq Mountain Formation in Saudi Arabia (Carrigan et al., 1995). This positive excursion possibly represents a major carbon cycle perturbation recognized elsewhere in both oceanic and terrestrial reservoirs. Bartolini et al. (1999) and Katz et al. (2005) report a large positive carbon isotope excursion in the middle Callovian and remaining positive until the Middle Oxfordian from the Atlantic Ocean. A broad Callovian - Oxfordian peak is seen also in the organic carbon isotope record of Nunn et al. (2009) from Scotland. Other late Jurassic marine successions are also characterized by positive carbon isotope excursions occurring during the Middle Oxfordian (Jenkyns 1996; Wierzbowski, 2004; Louis-Schmid et al. 2007). Louis-Schmid et al. (2007) for example, locate peak carbon isotope values within the Plicatilis and Transversarium ammonite zones (see also Jenkyns, 1996). Pearce et al. (2005) also describe a mid-Oxfordian positive carbon-isotope excursion recognised from fossil wood principally from Scotland. Notably the studies of Louis-Schmid et al. (2007) and Jenkyns (1996)

report little data from the Callovian – but when they do high positive ^{13}C values are also seen. In contrast, the belemnite isotope record of the Callovian–Oxfordian boundary in the Russian Platform, is described as being characterized by significant scatter and no temporal carbon isotope trend evident (Wierzbowski and Rogov, 2011).

Jurassic seawater paleotemperature reconstructions are frequently determined using the oxygen isotope composition of biogenic carbonate (e.g., Anderson et al. 1994; Dromart et al., 2003; Korte and Hesselbo, 2011). It is widely assumed that marine molluscs e.g., belemnites and oysters precipitate their rostra and shells in isotopic equilibrium with seawater (e.g., Anderson et al. 1994; Dromart et al., 2003; Price and Page, 2008; Nunn et al., 2009; Wierzbowski and Rogov, 2011; Pellenard et al., 2014). The equation of Anderson and Arthur (1983), and a δ value of −1‰ SMOW for an ice-free Earth, has typically been used. There is, however, much uncertainty regarding the −1‰ seawater value, for palaeotemperature reconstructions, because this value varies with changes in $\delta^{18}O_{seawater}$ (which can in turn be related to salinity) and ice-volume changes (Price and Teece, 2010; Pellenard et al. 2014). The modelling of Zhou et al., (2008) points to values at northern hemisphere temperate latitudes ranging from −1.0 and −2.0‰. A recent study looking at clumped isotopes and belemnites (Vickers et al. 2021) suggests that the equation of Kele et al. (2015), for slow-growing, abiotic calcites, when applied to well-preserved belemnite calcite, returns temperatures considerably warmer than the equation of Anderson and Arthur (1983) and δ^{18}Oseawater values within the expected range for open water to semi-enclosed basin setting (consistent with Zhou et al., 2008). That the $\delta^{18}O$ data from the belemnites, oysters and Gryphaea showing near similar tends through the examined interval suggests a consistency of the ambient waters affecting both the nektonic (belemnites) and benthic (oysters and Gryphaea) organisms. Evaluating the data presented here (Figs. 7, 8) and assuming a constant $\delta^{18}O_{seawater}$ value suggests a warm temperature shift of ~4 degrees from the Bajocian to Callovian (Peterborough Member,

Jason Zone). Follows is a cooling in the late Callovian and Oxfordian. The oyster and Gryphaea data show a similar pattern warming followed by cooling. Oxygen isotope thermometry based on shark tooth enamel (Dromart et al. 2003) has also been interpreted to indicate a severe cooling at the Middle-Late Jurassic transition. In the studies of Dromart et al. (2003) and Dera et al. (2011) seawater cooling is inferred to have begun in the Middle or Late Callovian. Notably our study suggests that the cooling (of up to 5 degrees) occurs within the Late Callovian (Athleta) and Early Oxfordian (Mariae) zones, after the positive carbon isotope excursion.

Late Jurassic (Callovian-Kimmeridgian) clumped isotope thermometry (Wierzbowski et al. 2018; Vickers et al. 2020, 2021) show near constant seawater temperatures across this interval, despite an accompanying shift to more negative $\delta^{18}O_{belemnite}$ values across the same interval. Rather than an increase in temperatures, the decrease in belemnite $\delta^{18}O$ values are interpreted as a decrease in the isotopic composition of seawater as a result of a reduced salinity and freshening (Wierzbowski et al. 2018). So, a decrease in $\delta^{18}O_{seawater}$ may account for some of the Oxfordian – Kimmeridgian warming observed in this study (Figs. 7, 8). A large decline of ~8 PSU is implied. There is unfortunately insufficient clumped isotope data to constrain temperatures across the Middle-Late Jurassic transition.

Palaeobiographical studies of ammonites by Dromart et al., (2003), suggests that in the Late Callovian, there was a southward excursion of Boreal Sea ammonites into warmer waters e.g., Kosmoceratidae readily populated Southern Europe (Lamberti Zone, Portugal). This migration of ammonite fauna into warmer waters, suggests a decline in sea surface temperatures during the Late Callovian. Furthermore, sequence stratigraphy studies have suggested there was a transgression peaking in the Middle Callovian – correlating with warmest temperatures, and a sea level low stand and regressive event in the Late Callovian–Early Oxfordian (e.g., turbidites in

315 Atlantic, the North Sea, Oman and Algeria) (Dromart et al., 2003) followed by mid-Oxfordian
316 maximum flooding (Husinec et al., 2022).

317 A correlation with the demise of carbonate production rates in the oceans during at the Callovian –
318 Oxfordian boundary (Donnadieu et al., 2011), could have increased seawater alkalinity and caused a
319 reduction in atmospheric CO_2, therefore generating a short-term cooling period (Wierzbowski et al.,
320 2013). Therefore, the positive $\delta^{13}C$ excursion, followed by a positive $\delta^{18}O$ shift peaking in the Late
321 Callovian and continuing into the early Oxfordian, as noted above could be associated with
322 enhanced carbon burial and cooling induced by carbon drawdown (e.g., Dromart et al., 2003; Nunn
323 and Price, 2010; Pellenard et al., 2014). Even allowing for some polar amplification, whether the
324 cooling at ~40°N was sufficient to see ice sheet formation (Dromart et al., 2003; Pellenard et al.,
325 2014) is questionable. For example, biogenic carbonate oxygen isotope records from the Russian
326 Platform, suggest that the southward ammonite fauna migrations in the Callovian and Oxfordian
327 and the presence of colder bottom waters, is the actually a result of changes in marine current
328 circulation due to the opening and closing of basins related to high/low stands during the Callovian
329 and Oxfordian (Wierzbowski et al., 2013).

330 **6. Conclusions**

331 The belemnite, oyster and Gryphaea samples provide the first stratigraphic analysis of $\delta^{18}O$ and
332 $\delta^{13}C$ isotope data at the Middle –Late Jurassic transition in Southern England, offer valuable
333 evidence regarding the prevailing palaeoclimatic conditions. Most samples are well-preserved.
334 Integration the results from this study with published $\delta^{18}O$ and $\delta^{13}C$ datasets, shows a negative shift
335 in $\delta^{18}O$, indicating a temperature rise (Bajocian-Middle Callovian) followed by more positive $\delta^{18}O$
336 values (a cooling of up to 5 degrees) occurring within the Late Callovian (Athleta) and Early
337 Oxfordian (Mariae) zones. This cooling agrees with earlier suggestions of a cooling episode at the

Middle –Late Jurassic transition, although such trends are less apparent in larger datasets (e.g., Dera et al. 2011). This cooling occurs after a prominent the positive carbon isotope excursion, possibly associated with enhanced organic carbon burial. A large positive carbon isotope excursion in the middle Callovian and remaining positive until the middle Oxfordian has also been observed by Bartolini et al. (1999), Katz et al. (2005) and Nunn et al. (2009) revealing a consistency in isotopic trends. Whether there was continental ice formation during this cooling episode is still debated (Wierzbowski and Rogov, 2011; Donnadieu et al. 2011). A cooling of 3-5 degrees at mid latitudes does not necessarily point to polar ice formation. If Jurassic polar climates were truly warm (e.g., Jenkyns et al., 2012; Vickers et al., 2019) such a degree of cooling would undoubtedly lead to cooler polar temperatures – but only with seasonal ice (e.g., Sellwood and Valdes, 2008).

Acknowledgements

We are grateful for the technical support provided by staff at the University of Plymouth. BH study visit to Plymouth, UK was supported by the Erasmus programme and the NRCFH (OTKA) project K135309.

References

Alberti, M., Fürsich, F.T., Pandey, D.K., Ramkumar, M. 2012. Stable isotope analyses of belemnites from the Kachchh Basin, western India: paleoclimatic implications for the Middle to Late Jurassic transition. Facies, 58, 261–278.

Anderson, T.F., Arthur, M.A., 1983. Stable isotopes of oxygen and carbon and their application to sedimentologic and environmental problems. In: Arthur, M.A., Anderson, T.F., Kaplan, I.R., Veizer, J., Land, L.S. (Eds.), Stable Isotopes in Sedimentary Geology: Society of Economic Paleontologists and Minerologists, Short Course Notes, 10, 1–151.

360 Anderson, T.F., Popp, B.N., Williams, A.C., Ho, L.Z., Hudson, J.D., 1994. The stable isotopic records of
361 fossils from the Peterborough Member, Oxford Clay Formation (Jurassic), UK:
362 paleoenvironmental implications. J. Geol. Soc. Lond., 151, 125–138.

363 Arkell, W.J. 1947. The Geology of the Country around Weymouth, Swanage, Corfe and Lulworth.
364 Memoir of the Geological Survey, 386 pp.

365 Banker, R.M.W., Sumner, D.Y., 2020 Structure and distribution of chalky deposits in the Pacific
366 oyster using x-ray computed tomography (CT). Scientific Reports, 10:12118

367 Barskov, I.S. Kiyashko 2000 Thermal regime variations in the Jurassic marine basin of the East
368 European Platform at the Callovian–Oxfordian boundary: evidence from stable isotopes in
369 belemnite rostra. Doklady Earth Sciences.

370 Bartolini, A., Baumgartner, P.O. & Guex, J. 1999. Middle and Late Jurassic radiolarian palaeoecology
371 versus carbon-isotope stratigraphy. Palaeogeography, Palaeoclimatology, Palaeoecology,
372 145, 43–60.

373 Brand U., Veizer, J 1980 Chemical Diagenesis of a Multicomponent Carbonate System--1: Trace
374 Elements. Jour. of Sediment. Petrol. 50, 1219–1236.

375 Callomon, J.H., Cope J.C.W. 1995. The Jurassic geology of Dorset. In Taylor, P. D (ed.), 1995. Field
376 Geology of the British Jurassic. Geological Society, London

377 Carrigan, W.J., Cole, G., Colling, E.L., Jones, P.J., 1995. Geochemistry of the Upper Jurassic Tuwaiq
378 Mountain and Hanifa Formation Petroleum Source Rocks of Eastern Saudi Arabia. Petroleum
379 Source Rocks, p. 67– 87.

380 Cope, J.C.W., 2016. Geology of the Dorset coast. Geologists' Association Guide No. 22. London: The
381 Geologists' Association. 2nd Edition.

382 Dera, G., Brigaud, B., Monna, F., Laffont, R., Pucéat, E., Deconinck, J.-F., Pellenard, P., Joachimski,
383 M.M. and Durlet, C. 2011. Climatic ups and downs in a disturbed Jurassic world. Geology, 39,
384 215–218.

385 Ditchfield, P.W., 1997. High northern palaeoaltitude Jurassic-Cretaceous palaeotemperature
386 variation: new data from Kong Karls Land, Svalbard. Palaeogeography, Palaeoclimatology,
387 Palaeoecology, 130, 163–175.

388 Donnadieu, Y., Dromart, G., Goddéris, Y., Pucéat, E., Brigaud, B., Dera, G., Dumas, C., Olivier, N.
389 2011. A mechanism for brief glacial episodes in the Mesozoic greenhouse.
390 Paleoceanography, 26, PA3212.

391 Dromart, G., Garcia, J. P., Picard, S., Atrops, F., Lécuyer, C. and Sheppard, S.M.F. 2003. Ice age at the
392 Middle–Late Jurassic transition? Earth and Planetary Science Letters, 213, 205–220.

393 Gradstein, F.M., Ogg, J.G., Schmitz, M.D. and Ogg, G.M. 2020. Geologic time scale 2020.
394 Amsterdam: Elsevier. 978–979.

395 Gröcke, D., Price, G.D., Ruffell, A., Mutterlose, J., Baraboshkin, E., 2003. Isotopic evidence for Late
396 Jurassic-Early Cretaceous climate change. Palaeogeography, Palaeoclimatology,
397 Palaeoecology, 202, 272–283.

398 Hendry, J.P., Kalin, R., 1997. Are oxygen and carbon isotopes of mollusc shells reliable palaeosalinity
399 indicators in marginal marine environments? A case study from the Middle Jurassic of
400 England. Journal of the Geological Society 154, 321–333.

401 House, M.R., 1993 Geology of the Dorset Coast 2nd Edition (1993) Geologists Association Guide

402 Hudson, J.D. and Martill, D.M., 1991. Fossils of the Oxford Clay. Palaeontological Association Field
403 Guide to Fossils, 4, 286 pp.

404 Husinec, A., Read, J.F., Prtoljan B., 2022. Middle and Late Jurassic record of sea-level, sequence
405 development, and carbon-isotope fluctuations, Tethyan Adriatic Carbonate Platform,
406 Croatia. Palaeogeography, Palaeoclimatology, Palaeoecology, 599, 1 111030.

407 Jenkyns, H.C. 1996. Relative sea-level change and carbon isotopes: data from the Upper Jurassic
408 (Oxfordian) of central and southern Europe. Terra Nova, 8, 75–85.

409 Jenkyns, H.C., Jones, C.E., Gröcke, D.R., Hesselbo, S.P. and Parkinson, D.N. 2002. Chemostratigraphy
410 of the Jurassic System: applications, limitations and implications for palaeoceanography.
411 Journal of the Geological Society, 159, 351–378.

412 Jenkyns, H.C., Schouten-Huibers, L., Schouten, S., Sinninghe Damsté, J. 2012. Warm Middle Jurassic-
413 Early Cretaceous high-latitude sea-surface temperatures from the Southern Ocean. Clim.
414 Past 8

415 Katz, M.E., Wright J.D., Miller, K.G., Cramer, B.S., Fennel, K., Falkowski, P.G. 2005 Biological
416 overprint of the geological carbon cycle. Marine Geology, 217, 323–338.

417 Kele, S., Breitenbach, S.F.M., Capezzuoli, E., Meckler A.N., Ziegler, M., Millan, I.M., Kluge, T., Deák,
418 J., Hanselmann, K., John, C.M., Yan H., Liu, Z., Bernasconi, S.M., 2015. Temperature
419 dependence of oxygen-and clumped isotope fractionation in carbonates: a study of
420 travertines and tufas in the 6–95C temperature range. Geochim. Cosmochim. Acta. 168,
421 172–192.

422 Kenig, F., Hayes, J.M., Popp, B.N., Summons, R.E. 1994 Isotopic biogeochemistry of the Oxford Clay
423 Formation (Jurassic), UK. Journal of the Geological Society, London, 151, 139–152.

424 Krenker, -N., Lindström, S., Bodin S. 2019. A major sea-level drop briefly precedes the Toarcian
425 oceanic anoxic event: implication for Early Jurassic climate and carbon cycle. Scientific
426 Reports 9, Article number: 12518.

427 Lécuyer, C., Picard, S., Garcia, J.-P., Sheppard, S.M.F., Grandjean, P., Dromart, G., 2003. Thermal
428 evolution of Tethyan surface during the Middle–Late Jurassic: evidence from 18O values of
429 marine fish teeth. Paleoceanography 18. doi:10.1029/2002PA000863

430 Li, Q., McArthur J., Doyle, P., Janssen, N., Leng, M.J., Müller, W., Reboulet, S., 2013. Evaluating
431 Mg/Ca in belemnite calcite as a palaeo-proxy. Palaeogeography, Palaeoclimatology,
432 Palaeoecology, 388, 98–108.

433 Louis-Schmid, B., Rais, P., Bernasconi, S.M., Pellenard, P., Collin, P.-Y., Weissert, H. 2007. Detailed
434 record of the mid-Oxfordian (Late Jurassic) positive carbon-isotope excursion in two
435 hemipelagic sections (France and Switzerland): A plate tectonic trigger? Palaeogeography,
436 Palaeoclimatology, Palaeoecology, 248, 459–472.

437 McArthur, J.M., Doyle, P., Leng, M.J., Reeves, K., Williams, C.T., Garcia-Sanchez, R., Howarth, R.J.
438 2007. Testing palaeo-environmental proxies in Jurassic belemnites: Mg/Ca, Sr/Ca, Na/Ca,
439 δ18O and δ13C. Palaeogeography, Palaeoclimatology, Palaeoecology, 252, 464–480.

440 Malchus, N., Aberhan, M., 1998. Transitional Gryphaeate/Exogyrate Oysters (Bivalvia: Gryphaeidae)
441 from the Lower Jurassic of Northern Chile. Journal of Paleontology, 72, 619–663.

442 Martin-Garin B., Lathuiliere B., Geister, J., Ramseyer, K., 2010 Oxygen isotopes and climatic control
443 of Oxfordian coral reefs (Jurassic, Tethys). Palaios, 25, 721–729.

444 Mettam, C., Johnson, A.L.A., Nunn E.V., Schöne, B.R., 2014. Stable isotope ($\delta^{18}O$ and $\delta^{13}C$)
445 sclerochronology of Callovian (Middle Jurassic) bivalves (*Gryphaea (Bilobissa) dilobotes*) and

belemnites (*Cylindroteuthis puzosiana*) from the Peterborough Member of the Oxford Clay Formation (Cambridgeshire, England): Evidence of palaeoclimate, water depth and belemnite behaviour. Palaeogeography, Palaeoclimatology, Palaeoecology, 399, 187–201.

Milliman, J.D. 1974. Marine Carbonates. Springer-Verlag, New York .

Nordt, L., Breecker, D., , J. 2021 Jurassic greenhouse ice-sheet fluctuations sensitive to atmospheric CO2 dynamics, Nature Geoscience

Nunn, E. V., Price, G. D., 2010. Late Jurassic (Kimmeridgian–Tithonian) stable isotopes ($\delta^{18}O$, $\delta^{13}C$) and Mg/Ca ratios: New palaeoclimate data from Helmsdale, north east Scotland. Palaeogeography, Palaeoclimatology, Palaeoecology. 292, 325–335.

Nunn E.V., Price G.D., Hart M.B., Page K.N., Leng M.J., 2009. Isotopic signals from Callovian - Kimmeridgian (Middle Upper Jurassic) belemnites and bulk organic carbon, Staffin Bay, Isle of Skye, Scotland. Journal of the Geological Society, 166, 633–664.

Padden, H., Weissert, H., De Rafelis, M., 2001. Evidence for Late Jurassic release of methane from gas hydrate. Geology 29, 223–226.

Palmer, T.J., Wilson, M.A. 1990. Growth of ferruginous oncoliths in the Bajocian (Middle Jurassic) of Europe. Terra Nova 2, 142-147.

Page, K.N., 1989. A stratigraphical revision for the English Lower Callovian. Proceedings of the Geologists Association, 100, 363–382.

Pearce C.R., Hesselbo, S.P., Coe, A.L. 2005. The mid-Oxfordian (Late Jurassic) positive carbon-isotope excursion recognised from fossil wood in the British Isles. Palaeogeography, Palaeoclimatology, Palaeoecology, 221, 343–357.

467 Pellenard, P., Tramoy, R., Pucéat, E., Huret, E., Martinez, M., Bruneau, L., Thierry, J. 2014. Carbon
468 cycle and seawater palaeotemperature evolution at the Middle–Late Jurassic transition,
469 eastern Paris Basin (France). Marine and Petroleum Geology, 53, 30–43.

470 Price, G.D. 2010. Carbon-isotope stratigraphy and temperature change during the Early–Middle
471 Jurassic (Toarcian–Aalenian), Raasay, Scotland, UK. Palaeogeography, Palaeoclimatology,
472 Palaeoecology, 285, 255–263.

473 Price, G.D., Page, K.N., 2008. A carbon and oxygen isotopic analysis of molluscan faunas from the
474 Callovian-Oxfordian boundary at Redcliff Point, Weymouth, Dorset: implications for
475 belemnite behaviour. Proceedings of the Geologists' Association, 119, 153–160.

476 Price, G. D., Rogov, M., 2009. An isotopic appraisal of the Late Jurassic greenhouse phase in the
477 Russian Platform. Palaeogeography, Palaeoclimatology, Palaeoecology, 273, 41–49.

478 Price, G.D., Teece, C. 2010. Reconstruction of Jurassic (Bathonian) palaeosalinity using stable
479 isotopes and faunal associations. J. Geol. Soc. London, 167, 1199–1208.

480 Price, G.D., Janssen, N.M.M., Martinez, M., Company, M., Vandevelde, J.H., Grimes, S.T. 2018. A
481 High-Resolution Belemnite Geochemical Analysis of Early Cretaceous (Valanginian-
482 Hauterivian) Environmental and Climatic Perturbations. Geochemistry, Geophysics,
483 Geosystems, 19, 3832–3843.

484 Price, G.D., Wilkinson, D., Hart, M.B., Page, K.N., Grimes, S.T. 2009. Isotopic analysis of coexisting
485 Late Jurassic fish otoliths and molluscs: Implications for upper-ocean water temperature
486 estimates. Geology, 37, 215–218.

Price, G.D., Hart, M.B., Wilby, P.R., Page, K.N., 2015. Isotopic analysis of Jurassic (Callovian) mollusks from the Christian Malford Lagerstätte (UK): implications for ocean water temperature estimates based on belemnoids. Palaios, 30, 645–654.

Rosales, I., Quesada, S., Robles, S., 2001 Primary and diagenetic isotopic signals in fossils and hemipelagic carbonates: the Lower Jurassic of northern Spain. Sedimentology, 48, 1149–1169.

Ruebsam, W., Al-Husseini, M.I., 2021. Orbitally synchronized late Pliensbachian–early Toarcian glacio-eustatic and carbon-isotope cycles. Palaeogeography, Palaeoclimatology, Palaeoecology, 577

Scotese, C.R., 2014. Atlas of Jurassic Paleogeographic Maps, PALEOMAP Atlas for ArcGIS, volume 4, The Jurassic and Triassic, Maps 32-42, Mollweide Projection, PALEOMAP Project, Evanston, IL.

Sellwood, B.W., Valdes, P., 2008. Jurassic climates. Proceedings of the Geologists' Association 119, 5– 17.

Vickers, M.L., Bajnai, D., Price, G.D., Linckens, J., Fiebig, J. 2019. Southern high-latitude warmth during the Jurassic–Cretaceous: New evidence from clumped isotope thermometry. Geology 47, 724–728.

Vickers, M.L., Fernandez, A., Hesselbo, S.P., Price, G.D., Bernasconi, S.M., Lode, S., Ullmann, C.V., Thibault, N., Hougård, I.W., and Korte, C., 2020, Unravelling Middle to Late Jurassic palaeoceanographic and palaeoclimatic signals in the Hebrides Basin using belemnite clumped isotope thermometry: Earth and Planetary Science Letters, 546, 116401.

508 Vickers, M.L., Bernasconi, S.M., Ullmann, C.V., Lode, S., Looser, N., Morales, L.G., Price, G.D., Wilby,
509 P.R., Hougård, I.W., Hesselbo, S.P. & Korte, C., 2021. Marine temperatures underestimated
510 for past greenhouse climate. Sci Rep 11, 19109.

511 Weissert, H. 1989. C-isotope stratigraphy, a monitor of paleoenvironmental change: a case study
512 from the early Cretaceous. Surveys in Geophysics 10, 1–61.

513 Wierzbowski, H., 2004. Carbon and oxygen isotope composition of Oxfordian – Early Kimmeridgian
514 belemnite rostra: palaeoenvironmental implications for Late Jurassic seas. Palaeogeography,
515 Palaeoclimatology, Palaeoecology, 203, 153–168.

516 Wierzbowski, H., Joachimski, M., 2007. Reconstruction of late Bajocian-Bathonian marine
517 palaeoenvironments using carbon and oxygen isotope ratios of calcareous fossils from the
518 Polish Jura Chain (central Poland). Palaeogeography, Palaeoclimatology, Palaeoecology, 254,
519 523–540.

520 Wierzbowski, H., Błażejowski, B., Tyborowski, D. 2019. Oxygen Isotope profiles of uppermost
521 Jurassic vertebrate teeth and oyster shells: A record of paleoenvironmental changes and
522 animal habitats. Palaios, 34, 585–599.

523 Wierzbowski, H., Dembicz, K., Praszkier, T., 2009. Oxygen and carbon isotope composition of
524 Callovian-Lower Oxfordian (Middle-Upper Jurassic) belemnite rostra from central Poland: A
525 record of a Late Callovian global sea-level rise? Palaeogeography, Palaeoclimatology,
526 Palaeoecology, 283, 182–194.

527 Wierzbowski, H., Rogov, M., 2011. Reconstructing the palaeoenvironment of the Middle Russian
528 Sea during the Middle–Late Jurassic transition using stable isotope ratios of cephalopod

shells and variations in faunal assemblages. Palaeogeography, Palaeoclimatology, Palaeoecology, 299, 250–264.

Wierzbowski, H., Rogov, M.A., Matyja, B.A., Kiselev, D. and Ippolitov, A. 2013. Middle–Upper Jurassic (Upper Callovian–Lower Kimmeridgian) stable isotope and elemental records of the Russian Platform: Indices of oceanographic and climatic changes. Global and Planetary Change, 7, 196–212.

Wierzbowski, H., Bajnai, D., Wacker, U., Rogov, M.A., Fiebig, J., Tesakova, E.M., 2018. Clumped isotope record of salinity variations in the Subboreal Province at the Middle–Late Jurassic transition. ScienceDirect Global and Planetary Change 167, 172–189.

Wright, J.K. 1986 A new look at the stratigraphy, sedimentology and ammonite fauna of the Corallian Group (Oxfordian) of South Dorset. Proceedings of the Geologists' Association, 97, 1–21.

Wright, J.K. 2014. A new section through the Corallian Group (Oxfordian, Upper Jurassic) rocks of Calne, Wiltshire, Southern England. Proceedings of the Geologists' Association, 125, 83–95.

Wright, J.K., 2016. The stratigraphy and geological setting of the Oxfordian Corallian Group around Steeple Ashton and Westbury, Wiltshire, U.K. Proceedings of the Geologists' Association, 127, 266–279.

Wright, J.K. and Cox, B.M., 2001. British Upper Jurassic Stratigraphy (Oxfordian to Kimmeridgian). Geological Conservation Review 21. Joint Nature Conservation Committee, Peterborough, 266.

549 Zhou, J., Poulsen, C.J., Pollard, D., White, T.S., 2008. Simulation of modern and middle Cretaceous
550 marine $\delta^{18}O$ with an ocean–atmosphere general circulation model. Paleoceanography 23,
551 PA3223.

552

553

554

555

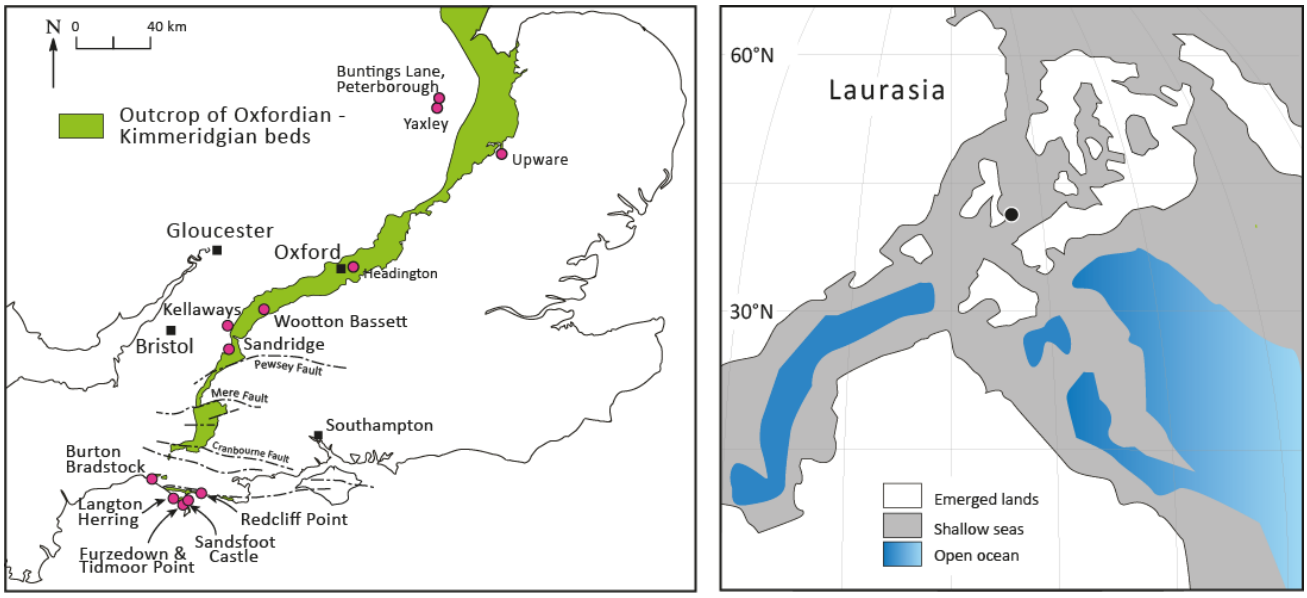

Figure 1 Outcrop map for the Lias Group in England and Wales and showing the location of Dorset, UK (after Wright and Cox, 2001). Late Jurassic (Oxfordian) palaeogeographic map modified from Scotese (2014).

562

563

564 Figure 2. Sampling locations across Dorset and Wiltshire illustrating the variable nature of

565 exposures. A. Well exposed Inferior Oolite in a large fallen block at Burton Cliff, Burton

Bradstock, Dorset. B. Oxford Clay exposed in low cliff exposures at Tidmoor Point, Fleet Lagoon, Dorset, C Fallen blocks of the Sandsfoot Grit Member Sandsfoot Castle, Weymouth, Dorset. D. The type locality of the Kellaways Formation, River Avon, west of Tytherton, Wiltshire, and E. Cliff exposure of the Callovian-Oxfordian boundary succession (Weymouth Member) at Redcliff Point near Weymouth, Dorset, UK.

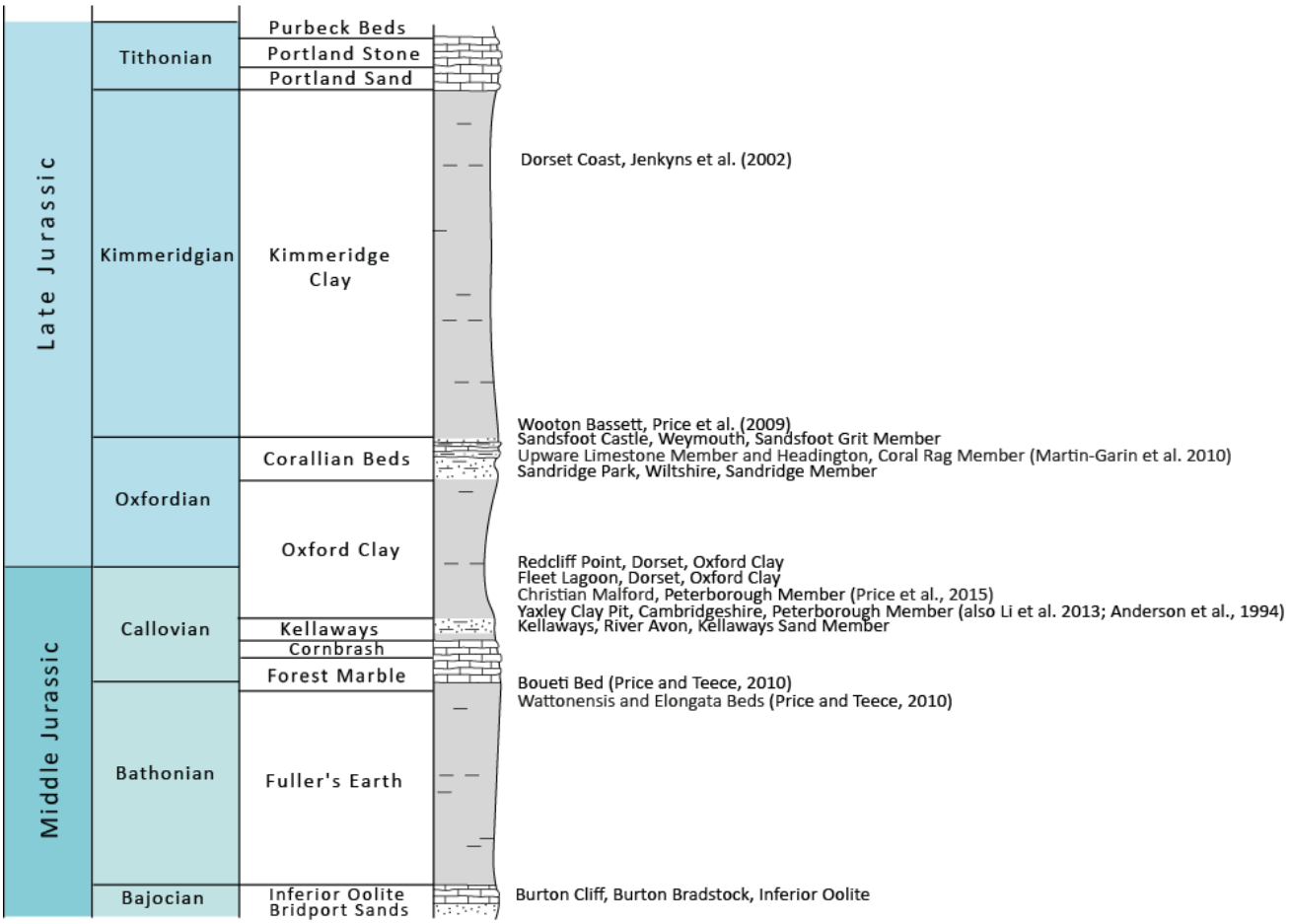

572

573 Figure 3. A summary of the Middle and Upper Jurassic stratigraphic succession of Dorset area

574 (modified from Wright, 1986; House 1993) with sampling (location) levels and published

575 sources of data.

576

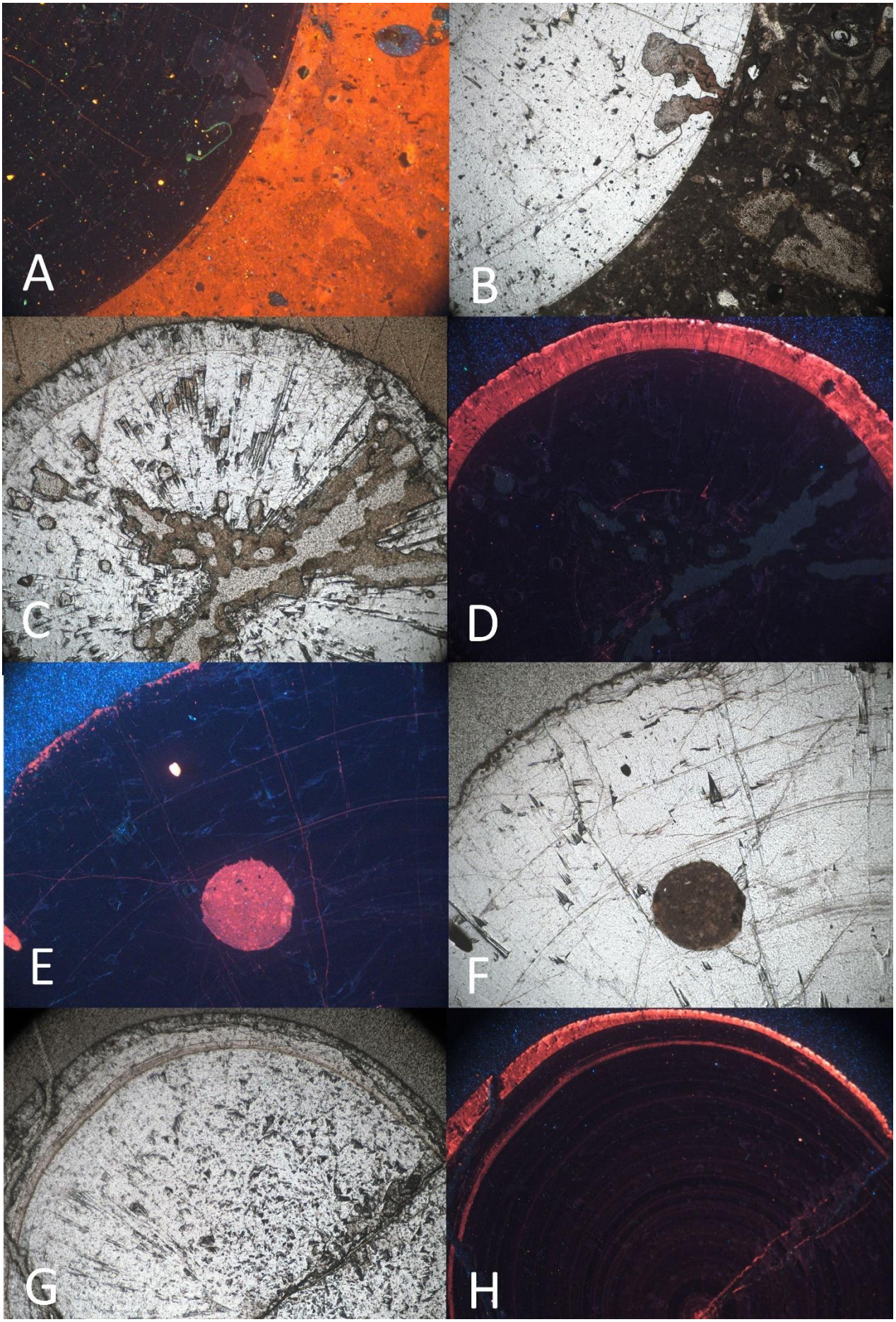

577

Figure 4 CL and plane polarised light photomicrographs (A, B) of non-luminescent rostrum within highly luminescent carbonate (sample BBRC1); plane polarised light and CL photomicrographs (C, D) non-luminescent rostrum with luminescent margin (Sample TPB2); (E, F) non-luminescent rostrum with luminescent sediment infilled boring (Sample BBSB1) and plane polarised light and CL photomicrographs (G, H) luminescent apical line area of rostrum, fracture and luminescent margin (Sample FDB12).

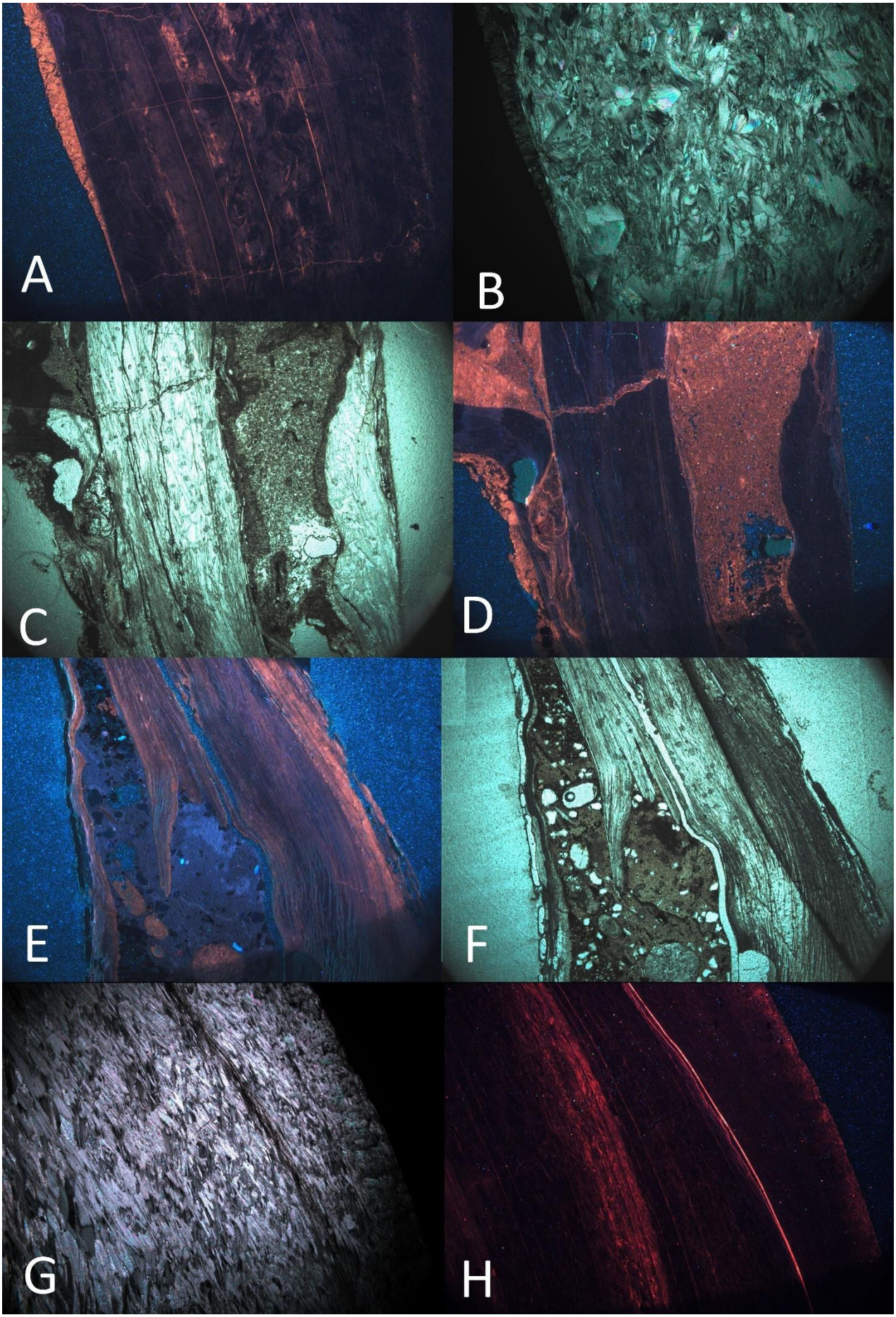

585

Figure 5. CL and crossed polarised light photomicrographs (A, B) of Gryphaea showing complex cross foliation, largely non-luminescent and thin luminescent fractures (sample FDG7); plane polarised light and CL photomicrographs (C, D) of non-luminescent oyster with strongly luminescent sediment and cement within interspersed chambers and luminescent sparry calcite fracture (sample TPO4); CL and plane polarised light photomicrographs (E, F) showing well-preserved largely non- luminescent foliated shells, with luminescent calcite along the outer shell margin, and sediment infilled interspersed lens shaped chambers (Sample SCO14) and crossed polarised light and CL photomicrographs (G, H) of Gryphaea showing complex cross foliation, largely non-luminescent and thin luminescent fractures (sample TPG6).

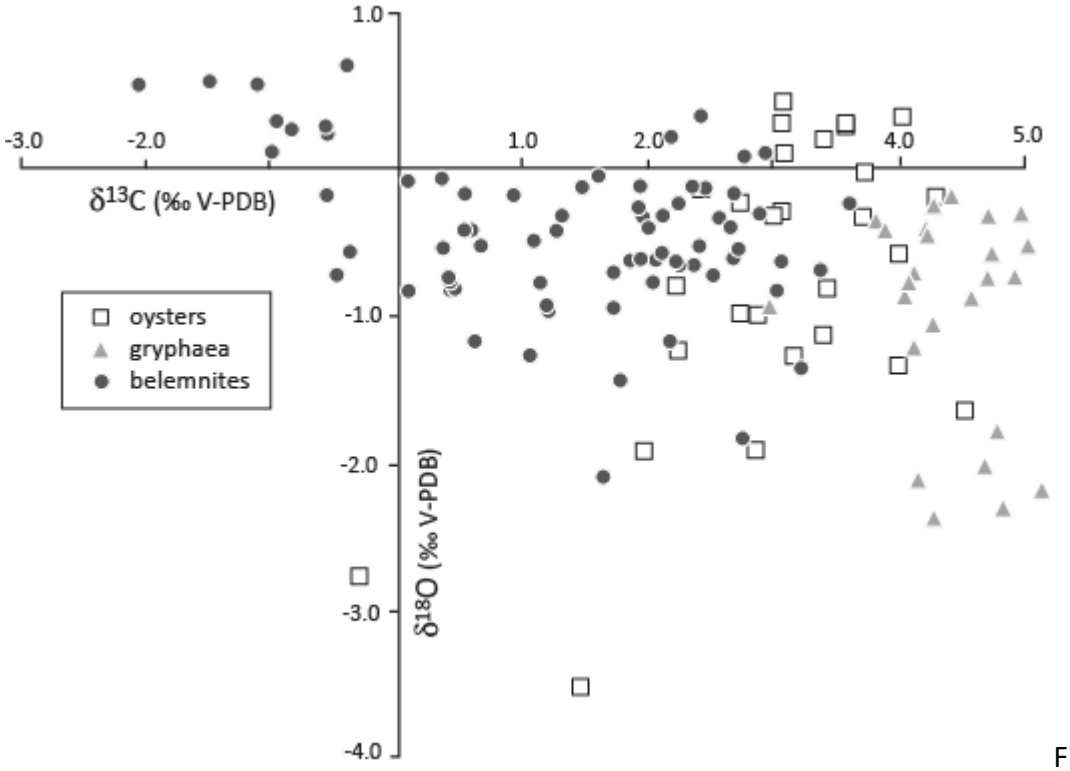

Figure 6. Cross plot of $\delta^{18}O$ and $\delta^{13}C$ data from the belemnite specimens, Gryphaea and oysters

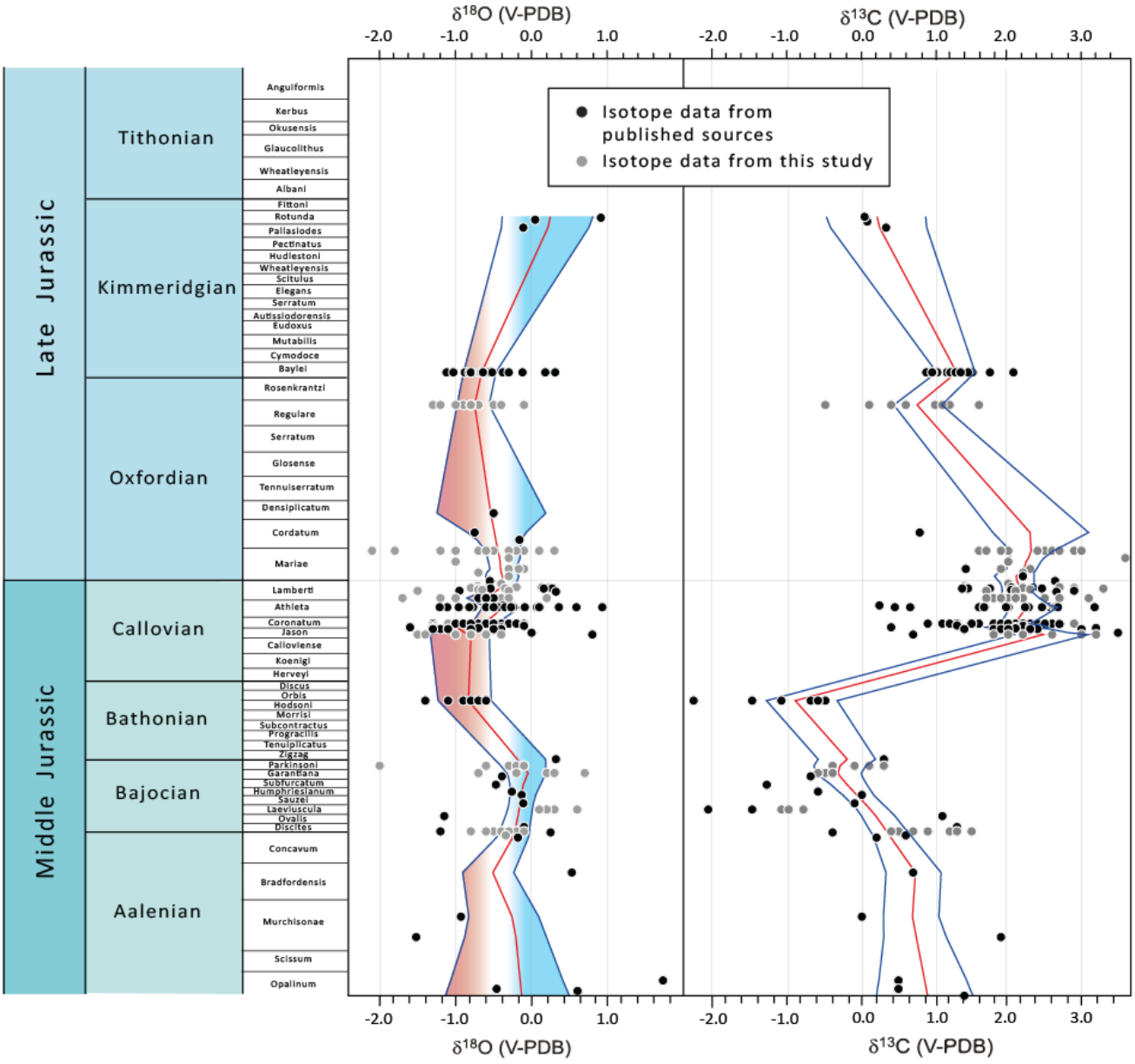

Figure 7 Belemnite $\delta^{18}O$ and $\delta^{13}C$ trends and LOESS curve fitting. Data are scaled to the GTS2020 timescale, based on ammonite zonation (from Wright and Cox 2001; House, 1993). The $\delta^{18}O$ curve has been coloured red to blue to indicate that more negative $\delta^{18}O$ may reflect warmer conditions, and more positive values with cooler conditions. Data presented is from this study and published sources noted in the text.

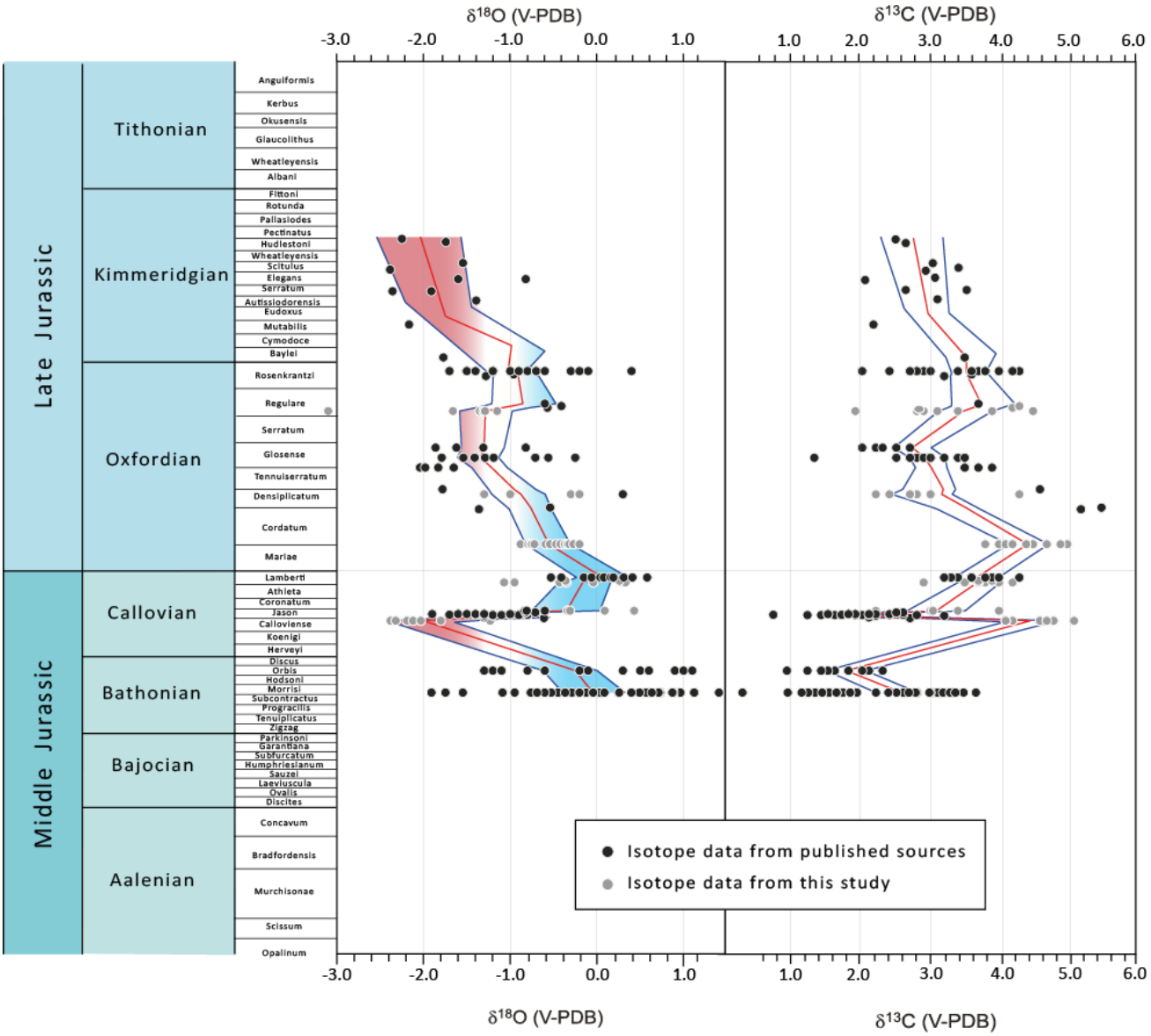

Figure 8. Oyster and Gryphaea $\delta^{18}O$ and $\delta^{13}C$ values trends and LOESS curve fitting. Data are scaled to the GTS2020 timescale, based on ammonite zonation (from Wright and Cox 2001; House, 1993). The $\delta^{18}O$ curve has been coloured red to blue to indicate that more negative $\delta^{18}O$ may reflect warmer conditions, and more positive values with cooler conditions. Data presented is from this study and published sources noted in the text.